

A HEADING CONSTRAINT CALIBRATION METHOD FOR LOW-END INERTIAL MEASUREMENT UNITS

Yizhou Xue¹, Xueli Guo¹, Zhenqi Zheng¹, You Li^{1,2} *

¹ State Key Laboratory of Information Engineering in Surveying, Mapping and Remote Sensing, Wuhan University, Wuhan, 430079, China - (aaaalien, guoxueli, zhengzhenqi, liyou)@whu.edu.cn

² Hubei LuoJia Laboratory, Wuhan, China

Commission III, WG III/1

KEY WORDS: IMU calibration Method, MEMS Inertial Sensors, Kalman Filtering, Pseudo-observation.

ABSTRACT:

The calibration result of the IMU has a strong impact on the accuracy of inertial navigation and its integration with other navigation techniques. Thus, how to efficiently obtain high-precision IMU calibration results is an important research problem for localization and motion tracking with consumer devices. To solve this problem, this paper proposes a handheld calibration method. Similar to our previous work, the pseudo observation is used to replace the measurement equation of the Kalman filter in the GNSS/INS loosely-coupled navigation algorithm. Compared to the existing online calibration algorithm, a more convenient data acquisition method is used, and the heading constraint information is added to assist in obtaining the calibration results of the IMU. To verify the proposed algorithm, a simulator is used to generate the heading updates with various precisions. The proposed algorithm shows the potential to estimate the vertical gyro bias, which does not converge in the existing calibration method, within around 0.5s when the accuracy of the heading's random error is 5 degrees. When the heading random error is 60 degrees, the vertical gyro bias can converge in about 6 seconds after rotation with the standard deviation of 121.7765 deg/h.

1. INTRODUCTION

In the related services of navigation and positioning, the global navigation satellite system (GNSS) can provide global, all-weather, high-precision positioning results in outdoor scenarios. However, in urban sections with elevated buildings such as tunnels and underground garages, the accuracy of the positioning results will be reduced or even lost. In this case, high-precision positioning results are usually obtained in combination with inertial measurement unit (IMU) data. In indoor scenarios, the IMU can provide reliable data around the clock, and in combination with other sensors, it can also provide better indoor positioning results.

With the advancement and development of microelectronics technology, IMU is also developing in the direction of small size, small weight, and low power consumption. Compared with traditional IMU, although its price is low and there are many application scenarios, its error also increases several orders of magnitude. To make better use of the micro-electromechanical systems (MEMS) IMU data, it is usually calibrated to obtain biases and scale factors errors (Jimenez et al. 2009). The biases and scale factors will change with time and temperature. Therefore, before data acquisition, it is generally necessary to calibrate the device to obtain the biases and scale factors errors. Therefore, how to easily and quickly obtain high-precision IMU data is an important research question. The calibration result of the IMU determines the accuracy of subsequent navigation using it.

Commonly used classical IMU calibration methods include the 6-position method, 12-position method, and 24-position method (Xiao et al. 2008), etc. To use such methods, the IMU data is collected under special conditions through equipment such as

turntables and cubes, and then the calibration parameters are calculated and obtained. Such approaches can provide accurate and reliable calibration results. However, for consumer devices such as smartphones and Internet-of-Things (IoT) devices (Poulose et al. 2019), it is not always affordable to use professional calibration equipment. Thus, it is necessary to use develop calibration methods that do not rely on calibration devices. There are existing in situ or online calibration methods for consumer-grade IMUs (Li et al. 2012); however, the latest online calibration method requires around 30 seconds for the gyro errors to converge. Meanwhile, it has weak observability on vertical gyro errors. Thus, new calibration methods are required to further improve calibration efficiency and enhance the observability of the vertical gyro.

This paper designs an algorithm to obtain IMU calibration results with heading information assistance. The algorithm obtains IMU data and other sensor data by hand-held motions, uses rotations within a limited range as pseudo observations, and uses the pseudo observations value instead of GNSS observations, which in the GNSS/INS loosely-coupled navigation algorithm (Falco et al. 2017). Add the heading information of other sensors to constrain and increase the observability of the vertical gyro. Meanwhile, the gyro and accelerometer biases in the IMU are calibrated together, using the Kalman filter algorithm. Furthermore, to analyze the algorithm performance and guide the calibration motion design, the observations in the navigation algorithm are calculated.

Therefore, the proposed IMU calibration method is different from the existing ones, which require special movements or professional equipment to initialize the equipment used in the corresponding scenarios. The goal of the proposed calibration

* Corresponding author Email: liyout@whu.edu.cn (You Li)

algorithm is to obtain the calibration results of the gyro and the accelerometer during a short period only by collecting the necessary data using a mobile phone or other devices.

2. METHODOLOGY

Compared with the traditional IMU calibration algorithm, the algorithm in this paper has the following advantages:

First, there is no need to use turntables, cubes, or other equipment to collect static and quasi-static data of the IMU under different attitudes, which reduces the difficulty of calibration data collection.

Second, taking the GNSS/INS integrated navigation algorithm as the main body, the concept of pseudo observations is introduced, and the three-axis accelerometer and the three-axis gyro can be calibrated with each other through the Kalman filter algorithm to obtain better calibration results.

Third, by adding heading observations, the divergence of the gyro heading data is further constrained, the observability of the vertical gyro is increased, and the convergence of the calibration results is accelerated.

2.1 Basic ideas

Under certain dynamic conditions, the GNSS/INS loosely-coupled navigation algorithm can compensate online for the biases and scale factors of the IMU (Hong et al. 2005). However, due to the possibility of GNSS data loss, and the consideration of the indoor environment. This paper uses constraints instead of GNSS measurements. As the IMU rotates around its measurement center, its position remains constant and its linear velocity is zero. Then it can be considered that the observed value under the constraint condition is $\hat{r}^n = \text{constant}$, $\hat{v}^n = 0$.

In the actual calibration process, the motion change of the IMU is reflected in the noise covariance matrix of the measurement equation in the Kalman filter.

Another rationale for this algorithm is that the output of the accelerometer can be used to calibrate the gyro (Fong et al. 2008). In the traditional accelerometer calibration algorithm, the gravity vector can provide the calculation data of the algorithm, and at the same time, the attitude information provided by the gyro can also assist in calculating the errors of the accelerometer.

In the GNSS/INS integrated navigation system, its observability largely depends on maneuvering (Lu et al. 2007). To obtain better calibration results, three-axis accelerometers and three-axis gyros should be fully stimulated by the corresponding motion.

For the existing online calibration algorithms, the observability of the vertical gyro is weak. On this basis, if there is the constraint of heading information, the errors of the gyro can be quickly converged in the calibration algorithm, and the efficiency of the algorithm can be improved.

Therefore, the motion mode of the data acquisition in this paper is shown in Figure 1. The rotation direction of the IMU coincides with the Z-axis, and it is fully rotated around the IMU measurement center to obtain the output data of the accelerometer and gyro. Different from the existing online calibration algorithm, this algorithm also needs to obtain constraint information, which comes from the heading information within the rotational motion range. For consumer devices such as smartphones and Internet-of-Things (IoT) devices, it can be extracted from data acquired by sensors such as cameras or magnetometers that are fixed to the IMU, and this process is not described in detail in this paper.

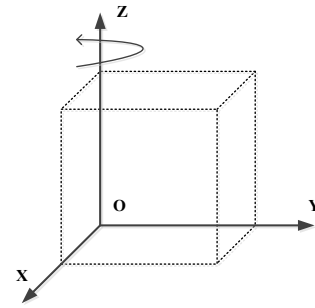


Figure 1. The rotations of IMU data collection.

2.2 Algorithm design

The overall flow of the calibration algorithm proposed in this paper is shown in Figure 2. The algorithm is based on the loosely-coupled GNSS/INS navigation algorithm (Wendel et al. 2004). First, input the collected accelerometer and gyro initial data into the INS mechanization to obtain the required information such as position, velocity, and attitude. Pseudo observations are introduced to replace GNSS position and velocity information. The state vector is constructed, and the pseudo observation information is input to the filter to correct the state vector (Welch et al. 1995). Using the heading information of the motion obtained from other sensors as a constraint, the state vector corrected by the pseudo observation value is further corrected, and the vertical gyro information is constrained to obtain the final accelerometer and gyro calibration results.

The mechanical arrangement of the IMU can refer to (Shin 2005), which will not be described in detail here.

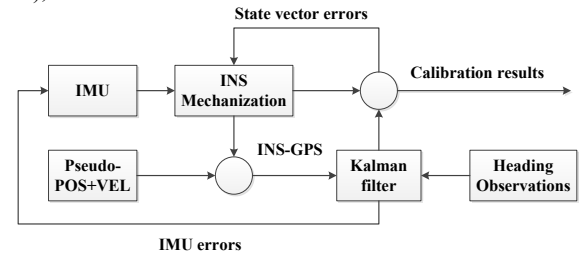


Figure 2. The overall process of the calibration algorithm.

2.2.1 Sensor error models

The main influence errors that need to be considered when using MEMS-IMU sensors in different scenarios are mainly the biases and the scale factors, which are mainly affected by factors such as temperature.

Among the two, the biases have a greater influence, so only the errors generated by the biases are considered in this paper, and the complete error model will be considered in the follow-up research (Aggarwal et al. 2008).

Therefore, considering the effect of the biases on the output of the accelerometer and gyro, the error equations for the accelerometer and gyro are as follows:

$$\delta f^b = b_a + \text{diag}(\tilde{f}^b) \delta s_a + w_a \quad (1)$$

$$\delta \omega_{ib}^b = b_g + \text{diag}(\tilde{\omega}_{ib}^b) \delta s_g + w_g \quad (2)$$

where δf^b and $\delta \omega_{ib}^b$ are the error vectors of specific force and angular velocity. b_a and b_g are the biases vector of the accelerometers and gyros. w_a and w_g are the sensor noises. δs_a and δs_g are the scale factor errors vector of the accelerometers and gyros. \tilde{f}^b is the measured specific force.

$\tilde{\omega}_{ib}^b$ is the measured angular rate. *diag* refers to converting the vector to a diagonal matrix. Since the time spent in the calibration process is generally short. In this process, the biases errors and scale factor errors can be regarded as a random constant that does not change with time (Maybeck 1982).

2.2.2 Kalman filter system model

The Kalman filter system model used in this paper is derived based on the paper(Shin 2005).

$$\delta \dot{r}^c = -\omega_{ec}^c \times \delta r^c + \delta v^c \quad (3)$$

$$\delta \dot{v}^c = F_{vr} \delta r^c - (2\omega_{ie}^c + \omega_{ec}^c) \times \delta v^c + f^c \times \psi + C_b^p \delta f^b \quad (4)$$

$$\dot{\psi} = -(\omega_{ie}^c + \omega_{ec}^c) \times \psi - C_b^p \delta \omega_{ib}^b \quad (5)$$

where δr^c and δv^c are the error of position and velocity, respectively. ψ is the conversion angle between p-frame (The platform frame is the frame in which the transformed acceleration from the accelerometers and angular rates from the gyros are resolved (Scherzinger 1996)) and c-frame (The computer frame is the frame that the INS computer assumes to be the true navigation frame (Scherzinger 1996)). C_b^p is the direction cosine matrix of coordinate transformation from b-frame to p-frame. f^c is the projection of specific force on the c-frame. ω_{ie}^c is the projection of the angular velocity of the earth's rotation in the c-frame. ω_{ec}^c is the projection of the c-frame relative the e-frame's motion in the c-frame.

$$F_{vr} = \text{diag}\left(\left[-\frac{g}{R_M + h} \quad -\frac{g}{R_N + h} \quad \frac{2g}{R + h}\right]\right) \quad (6)$$

where R_M is the radius of the meridian circle. R_N is the radius of curvature in the prime vertical. R is the Gaussian radius of curvature. g is the local gravity value, and h is the corresponding altitude.

For the scenario in this paper, (3) to (5) are correspondingly simplified, and the process will not be described in detail in this paper. For the specific process, please refer to(Li et al. 2012).

$$\delta \dot{r}^n = \delta v^n \quad (7)$$

$$\delta \dot{v}^n = f^n \times \psi + C_b^p \delta f^b \quad (8)$$

$$\dot{\psi} = -C_b^p \delta \omega_{ib}^b \quad (9)$$

2.2.3 Kalman filter measurement Model

In this paper, the pseudo observations are used as the measurement equation of the Kalman filter, and either pseudo-velocity or pseudo-position can be used.

$$\hat{v}^n = \delta v^n + n_v \quad (10)$$

$$\hat{r}^n - \tilde{r}^n = \delta r^n + n_r \quad (11)$$

with $\tilde{r}^n = \text{constant}$

where \hat{v}^n and \hat{r}^n are velocity and position vectors predicted by the INS mechanization. \tilde{r}^n is the observation vector of the proposed pseudo observation. δv^n and δr^n are represent the velocity errors and position errors, respectively. n_v and n_r represent the measurement noises of proposed pseudo-velocity and pseudo-position, respectively.

2.2.4 Heading observation

To increase the observability of the vertical gyro, this paper introduces the heading information to correct the state vector.

$$\hat{\psi}_{heading} - \tilde{\psi}_{heading} = \delta \psi_{heading} \quad (12)$$

where $\hat{\psi}_{heading}$ is the heading angle predicted by the INS mechanization. $\tilde{\psi}_{heading}$ is the heading angle measurement obtained by other sensors. $\delta \psi_{heading}$ represents the heading error.

2.2.5 Setting of the Kalman filter parameters

The setting of the Kalman filter parameters can refer to (Li et al. 2012), which will not be described in detail here.

According to the addition of heading information, it is necessary to consider the setting of parameters related to heading constraints. The measurement noise covariance matrix of the acquired heading angle R_h .

$$R_h = \text{diag}(\text{sigma}(\text{heading})^2) \quad (13)$$

where the exact value of R_h cannot be directly obtained, so experiences are usually set. And the experiences are manually adjusted according to the experimental results to obtain the best R_h .

3. SIMULATION TESTS AND RESULTS

To verify the feasibility of the calibration algorithm in this paper, a simulator is used to generate the IMU data required by the calibration algorithm. Using the simulator to obtain the test data, the true value of the navigation information can be obtained. Adding the required error to the navigation information, other interference factors can be greatly reduced. (Zampella et al. 2011).

3.1 Simulation analysis method

The simulator model used in this paper is shown in Figure 3. The part in the red box is the input, and the part in blue is the output data of the simulator, which is the output of the true information of reference navigation (i.e., position, velocity, and attitude), GNSS measurement information, and IMU output information respectively.

The simulator uses the artificially set initial navigation information, as well as the angular velocity and acceleration true value information generated by the set trajectory, and inputs it into the navigation mechanical arrangement algorithm to infer the navigation truth value at each subsequent time. The actual navigation information can be obtained by adding artificially set errors to the obtained truth information.

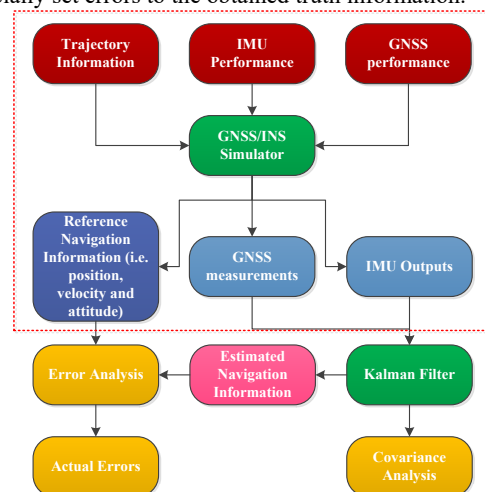


Figure 3. The diagram integrated navigation simulation and solution.

3.2 Simulation Tests

The motion trajectory of the calibration data is shown in Table 1.

Time(Sec)	Motion description
1-10	Keep static
10-20	Turn 360 degrees
20-30	Keep static

Table 1. Simulated calibration motions.

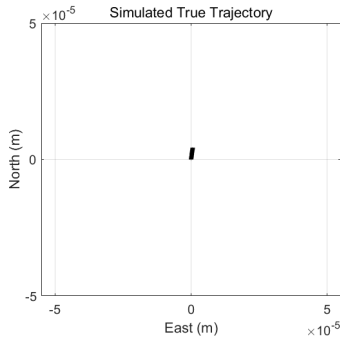


Figure 4. Simulated true trajectory.

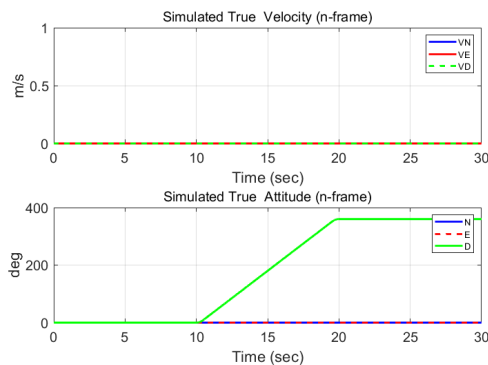


Figure 5. Simulated velocity and attitudes.

Through this motion trajectory, the reference navigation information and the true value of the IMU output can be obtained. As shown in Figure 4 and Figure 5, its true position and true velocity changes are approximately zero.

Based on the true value of the IMU output, according to (1) and (2), a series of simulation data can be obtained by adding typical consumer-grade errors. By adding random errors to the real heading data, the actual heading data obtained by other sensors can be simulated.

3.3 Calibration results and analysis

To more realistically simulate the application of the sensor related to the heading, this paper adds different errors to the real heading data.

The heading model is as follows:

$$\tilde{\psi}_{heading} = \psi_{heading} + b_h + w_h \quad (14)$$

where $\tilde{\psi}_{heading}$ is the heading angle measurement obtained by heading sensors. $\psi_{heading}$ is the true value of heading information. b_h is the static error of the heading sensors. w_h are the sensor noises.

In this paper, we set the value b_h to 0 and thought the sensor noises are gaussian white noise. The standard deviation of white noises are set to 5 degrees, 15 degrees, 30 degrees, and 60 degrees, respectively. The setting of other parameters can refer to (Li et al. 2012), which will not be described in detail here.

3.3.1 Statistical display of experimental results

For the above-mentioned four kinds of heading information with different precisions, this paper designs three different $R_h = \text{diag}(\text{sigma}(\text{heading})^2)$ for experiments. After obtaining multiple sets of experimental results, this paper uses the standard deviation and the root mean square value as statistical characteristics for evaluation. The statistical data is defined as the calibration result data from the convergence time of the algorithm to the end time.

The selection of convergence points refers to the following conditions:

- (1) Taking the calibration results from 20 s to 30 s when the rotation motion stops as a sample, calculate the mathematical expectation and standard deviation of the sample, and the difference between the convergence point and the expectation should not exceed twice the standard deviation.
- (2) Taking the convergence point as the center, select 20 data including the convergence point, and the variation of the data within this range should not be over the specified threshold.

The overall situation of the experimental results is shown in Figure 6.

Experiments show that the algorithm in this paper has good feasibility. For the x-axis and y-axis, the average value of the standard deviation of the accelerometer's biases are 385.752 μg and 424.616 μg , and the average value of the standard deviation of the gyro's biases are 23.5502 deg/h and 31.6084 deg/h, which have good precision.

For the bias error of the z-axis gyro, the average value of multiple sets of data is 292.6624 deg/h, which is basically in line with the accuracy of using.

The standard deviation of the z-axis bias of the accelerometer has a static error of about 7000 μg . The reason may be as follows. In the data acquisition designed in this paper, only the rotation of the z-axis is performed, and the scale factors error of the z-axis cannot be well estimated and constrained. Therefore, the scale factors error is compensated for the biases error of the z-axis. Because the x-axis and the y-axis have no rotation, the corresponding scale factor error does not affect the respective results.

For specific experimental results, please refer to sections 3.3.2-3.3.6.

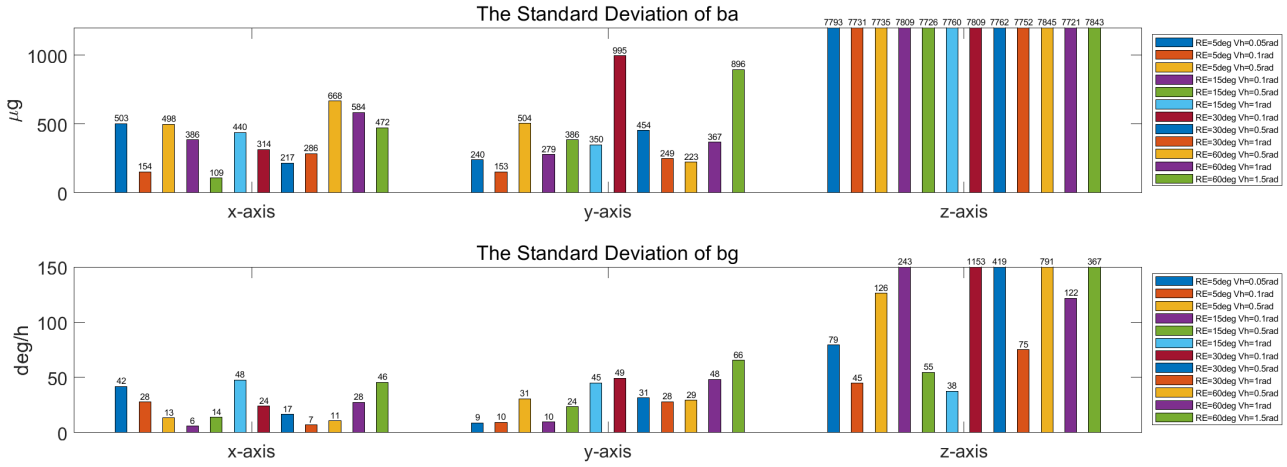


Figure 6. The standard deviation of bias.

3.3.2 No Heading information

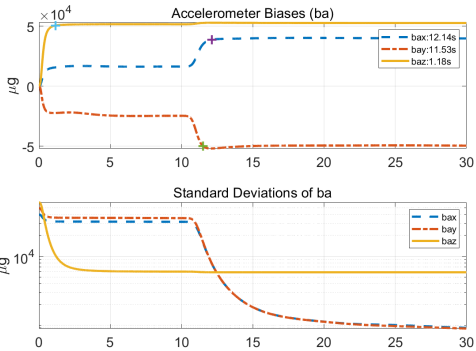


Figure 7. Accelerometer calibration results without heading information.

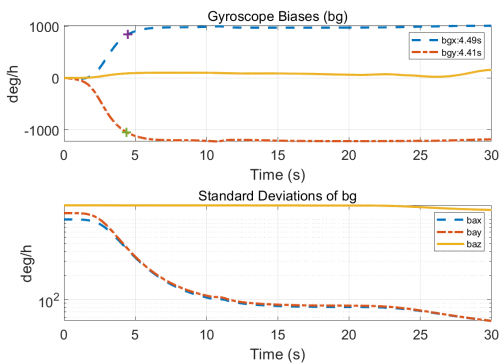


Figure 8. Gyro calibration results without heading information.

In this section, the value of $\sigma(\text{heading})$ is 100 radii, which is used to replace the situation where heading information is not available. In this case, the algorithm in this paper degenerates into an online calibration algorithm. Because of its local gravity vector, the z-axis bias of the accelerometer can converge in the initial one to two seconds, and the x-axis and y-axis gradually converge within two to four seconds after the IMU rotates. According to the statistical results of the standard deviation and the root mean square value, the calculated biases results of the x-axis and y-axis of the accelerometer are better than the results of the z-axis. As shown in Figure 8, although the results of the

x-axis and y-axis of the gyro converge to a good value within 5 seconds, the gyro's bias error of the z-axis cannot converge. The existing online calibration algorithm cannot obtain a complete gyro calibration result under this condition.

To obtain the complete gyro calibration results, heading information is used to assist in correcting calibration results, and the relevant experiments display in 3.3.3 to 3.3.6 sections.

3.3.3 The standard deviation of the heading's random error is 5 degrees

This section uses the heading information with an error of 5 degrees to implement the algorithm. Because R_h has no exact value, set $\sigma(\text{heading})$ to 0.05, 0.1, and 0.5 radii for experiments.

The statistical results of each group are shown in Table 2 and Table 3.

Accelerometer	0.05rad	0.1rad	0.5rad
Convergence time (s)			
x-axis	12.69	12.75	12.46
y-axis	13.87	13.44	12.28
z-axis	1.21	1.21	1.17
STD (μg)			
x-axis	502.63	153.55	497.54
y-axis	239.51	153.19	504.08
z-axis	7792.53	7730.71	7734.53
RMS (μg)			
x-axis	40472.91	40057.46	40218.69
y-axis	49876.12	49879.33	49618.30
z-axis	52234.97	52296.21	52291.93

Table 2. The statistics of accelerometer calibration results.

Gyroscope	0.05rad	0.1rad	0.5rad
Convergence time (s)			
x-axis	7.69	6.07	4.71
y-axis	7.69	7.29	4.62
z-axis	10.48	10.52	15.21
STD (deg/h)			
x-axis	41.99	27.86	13.41
y-axis	8.85	9.53	30.81
z-axis	79.45	36.77	126.17
RMS (deg/h)			
x-axis	958.34	976.03	997.72
y-axis	1195.71	1204.73	1171.31
z-axis	1436.19	1519.52	1623.24

Table 3. The statistics of gyro calibration results.

where the calibration results under the condition of 0.1 radii are better, and the calibration results are shown in Figures 9, 10. While maintaining a short convergence time, its standard deviation is also small.

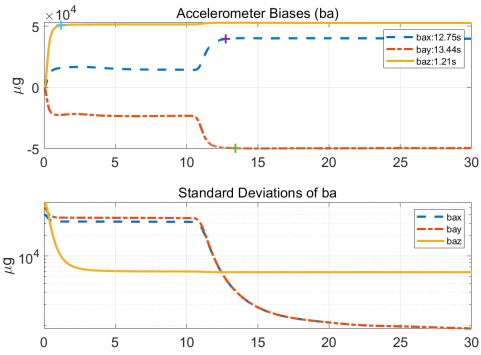


Figure 9. Accelerometer calibration results without heading information.

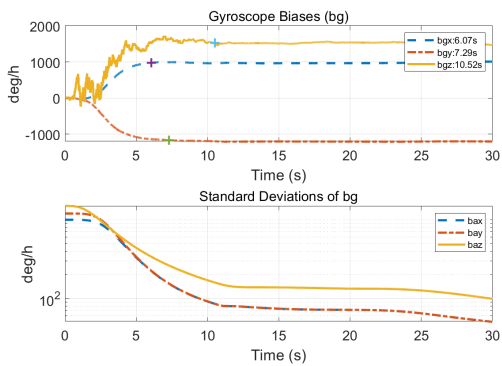


Figure 10. Gyro calibration results without heading information.

3.3.4 The standard deviation of the heading’s random error is 15 degrees

This section uses the heading information with an error of 15 degrees to implement the algorithm. Setting the $\sigma(\text{heading})$ to 0.1, 0.5, and 1 radius for experiments, and the statistical results of each group are shown in Table 4 and Table 5.

Accelerometer	0.1rad	0.5rad	1rad
Convergence time (s)			
x-axis	12.84	12.00	12.38
y-axis	12.91	11.77	12.13
z-axis	1.23	1.18	1.18
STD (μg)			
x-axis	385.50	108.78	439.65
y-axis	278.71	385.64	349.83
z-axis	7808.99	7726.03	7759.88
RMS (μg)			
x-axis	39680.13	40000.81	40157.37
y-axis	49726.44	50082.75	50254.77
z-axis	52212.89	52296.76	52262.17

Table 4. The statistics of accelerometer calibration results.

Gyroscope	0.1rad	0.5rad	1rad
Convergence time (s)			
x-axis	6.30	9.01	11.69
y-axis	7.96	10.73	11.69
z-axis	10.27	15.94	19.14
STD (deg/h)			
x-axis	5.99	13.83	47.74
y-axis	9.60	23.62	44.97
z-axis	242.56	54.35	37.73
RMS (deg/h)			
x-axis	1004.05	1010.02	954.00
y-axis	1208.20	1178.09	1156.12
z-axis	1335.10	1480.66	1478.87

Table 5. The statistics of gyro calibration results.

where the calibration results under the condition of 0.5 radii are better, and the calibration results are shown in Figures 11,12. Although its convergence time is longer than 0.1 radii, the standard deviation of its vertical gyro is better than the other two cases.

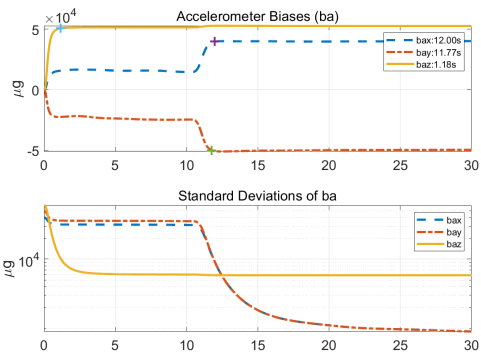


Figure 11. Accelerometer calibration results without heading information.

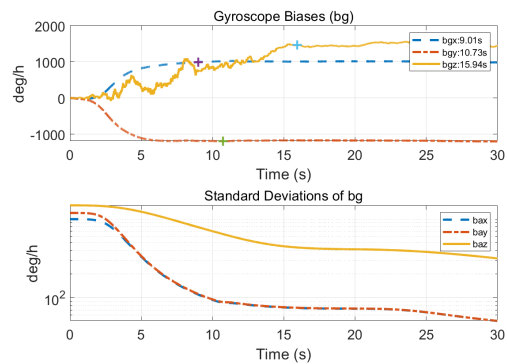


Figure 12. Gyro calibration results without heading information.

3.3.5 The standard deviation of the heading’s random error is 30 degrees

This section uses the heading information with an error of 30 degrees to implement the algorithm. Setting the $\sigma(\text{heading})$ to 0.1, 0.5, and 1 radius for experiments, and the statistical results of each group are shown in Table 6 and Table 7.

Accelerometer	0.1rad	0.5rad	1rad
Convergence time (s)			
x-axis	11.95	12.34	12.33
y-axis	11.71	12.30	12.32
z-axis	1.24	1.22	1.20
STD (ug)			
x-axis	314.03	216.57	285.61
y-axis	995.10	454.22	248.75
z-axis	7809.17	7761.72	7752.34
RMS (ug)			
x-axis	40222.47	40043.70	39764.79
y-axis	50892.49	49623.70	50205.01
z-axis	52202.89	52273.13	52274.96

Table 6. The statistics of accelerometer calibration results.

Gyroscope	0.1rad	0.5rad	1rad
Convergence time (s)			
x-axis	5.21	11.29	14.07
y-axis	6.27	9.46	11.31
z-axis	12.05	11.84	21.08
STD (deg/h)			
x-axis	24.03	16.74	7.13
y-axis	49.20	31.4	27.99
z-axis	1153.20	419.30	75.13
RMS (deg/h)			
x-axis	1006.58	983.74	994.11
y-axis	1163.44	1230.68	1173.47
z-axis	416.41	1906.37	1552.70

Table 7. The statistics of gyro calibration results.

where the calibration results under the condition of 1 radius are better, and the calibration results are shown in Figures 13,14. Although the convergence time of its gyro calibration results is longer than that of the other two cases, the standard deviation of its three-axis gyro is much lower than that of the other two cases.

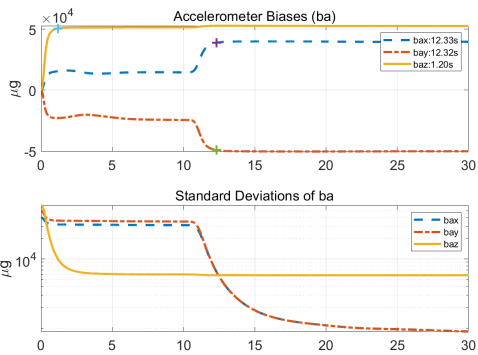


Figure 13. Accelerometer calibration results without heading information.

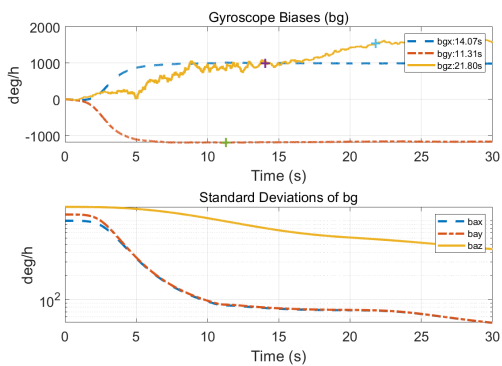


Figure 14. Gyro calibration results without heading information.

3.3.6 The standard deviation of the heading's random error is 60 degrees

This section uses the heading information with an error of 60 degrees to implement the algorithm. Setting the $\sigma(\text{heading})$ to 0.5, 1, and 1.5 radii for experiments, and the statistical results of each group are shown in Table 8 and Table 9.

Accelerometer	0.5rad	1rad	1.5rad
Convergence time (s)			
x-axis	16.24	11.88	12.12
y-axis	13.11	12.30	11.67
z-axis	1.19	1.24	1.23
STD (ug)			
x-axis	668.22	584.47	472.42
y-axis	223.03	367.47	895.79
z-axis	7845.26	7720.60	7842.60
RMS (ug)			
x-axis	39336.50	40508.72	40446.31
y-axis	49787.46	49674.38	50758.60
z-axis	52170.97	52311.00	52169.93

Table 8. The statistics of accelerometer calibration results.

Gyroscope	0.5rad	1rad	1.5rad
Convergence time (s)			
x-axis	9.59	12.30	11.35
y-axis	8.25	10.49	11.04
z-axis	15.56	16.03	15.81
STD (deg/h)			
x-axis	10.74	27.55	45.54
y-axis	29.27	48.38	65.62
z-axis	790.61	121.77	366.55
RMS (deg/h)			
x-axis	997.31	1026.32	956.57
y-axis	1225.06	1247.58	1136.04
z-axis	2282.86	1574.92	1812.69

Table 9. The statistics of gyro calibration results.

where the calibration results under the condition of 1 radius are better, and the calibration results are shown in Figures 15, 16.

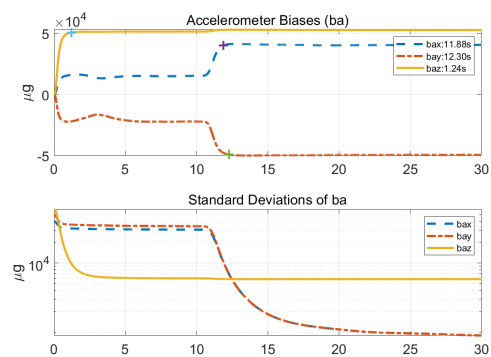


Figure 15. Accelerometer calibration results without heading information.

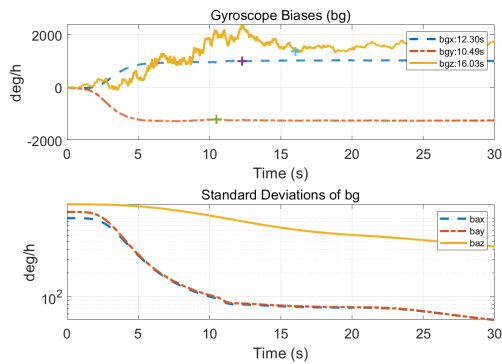


Figure 16. Gyro calibration results without heading information.

4. CONCLUSION

According to the results of ten groups of experimental data in section 3, the conclusion is as below:

- (1) Due to the weak observability, the calibration result of the vertical gyro does not converge. After adding the heading information for constraints, the complete IMU bias error result can be obtained, which shows the feasibility of this algorithm. According to the statistical characteristics in section 3.3.1, the average value of the standard deviation of the x-axis and y-axis accelerometer's biases are 385.752 ug and 424.616 ug, and the average value of the standard deviation of the gyro's biases are 23.5502 deg/h, 31.6084 deg/h, and 292.6624 deg/h which have good precision.
- (2) Although the addition of heading information makes up for the shortcomings of the existing calibration algorithms, the selection of $\sigma(\text{heading})$ is also a relatively important issue. When the random errors of heading information are 5 degrees, 15 degrees, 30 degrees, and 60 degrees, respectively, the corresponding optimal $\sigma(\text{heading})$ values are 0.1 radii, 0.5 radii, 1 radius, and 1 radius. It provides a reference for the fusion of heading information from different sensors in the follow-up research.
- (3) When the accuracy of the heading information is higher, the calibration results of the vertical gyro converge faster. In section 3.3.3, when $\sigma(\text{heading})$ is selected as 0.05 radii and 0.1 radii, the vertical gyro data begins to converge within 0.5s after the start of the rotation, but with the increase of heading information error, the convergence time also increases. In section 3.3.6, the convergence time is greater than 15s.
- (4) In the data acquisition designed in this paper, only the rotation of the z-axis is performed, the x-axis and the y-axis have no motion, and the corresponding scale factor error does not affect the respective results. For the z-axis, the standard deviation of the accelerometer has a static error of about 7000 ug. The reason may be as follows, the scale factors error is compensated for the biases error of the z-axis, and the scale factors error of the z-axis cannot be well estimated and constrained. The algorithm or data acquisition method needs to be improved in the future to avoid the recurrence of this situation in actual use.

ACKNOWLEDGEMENTS

This work was supported in part by the Major Basic Research Project (5140503A0301), the National Natural Science Foundation of China (42174050), the Provincial and Municipal "Double First-Class" Construction Project (600460035), and the Hubei Luojia Laboratory Special Fund.

REFERENCES

- Aggarwal, P., et al. (2008). "A standard testing and calibration procedure for low cost MEMS inertial sensors and units." *The Journal of Navigation* **61**(2): 323-336.
- Falco, G., et al. (2017). "Loose and tight GNSS/INS integrations: Comparison of performance assessed in real urban scenarios." *Sensors* **17**(2): 255.
- Fong, W., et al. (2008). "Methods for in-field user calibration of an inertial measurement unit without external equipment." *Measurement Science and Technology* **19**(8): 085202.
- Hong, S., et al. (2005). "Observability of error states in GPS/INS integration." *IEEE Transactions on Vehicular Technology* **54**(2): 731-743.
- Jimenez, A. R., et al. (2009). *A comparison of pedestrian dead-reckoning algorithms using a low-cost MEMS IMU*. 2009 IEEE International Symposium on Intelligent Signal Processing, IEEE.
- Li, Y., et al. (2012). "An in situ hand calibration method using a pseudo-observation scheme for low-end inertial measurement units." *Measurement Science and Technology* **23**(10).
- Lu, Z.-d., et al. (2007). "In-flight calibration method for SINS." *Journal of Chinese Inertial Technology* **4**(2): 136-138.
- Maybeck, P. S. (1982). *Stochastic models, estimation, and control*, Academic press.
- Poulose, A., et al. (2019). "An indoor position-estimation algorithm using smartphone IMU sensor data." *IEEE Access* **7**: 11165-11177.
- Scherzinger, B. M. (1996). *Inertial navigator error models for large heading uncertainty*. Proceedings of Position, Location and Navigation Symposium-PLANS'96, IEEE.
- Shin, E.-H. (2005). "Estimation techniques for low-cost inertial navigation." *UCGE report* **20219**.
- Welch, G., et al. (1995). "An introduction to the Kalman filter."
- Wendel, J., et al. (2004). "Tightly coupled GPS/INS integration for missile applications." *Aerospace Science and Technology* **8**(7): 627-634.
- Xiao, L.-x., et al. (2008). "Research on the high accuracy rapid test method of IMU." *Journal of Astronautics* **1**: 030.
- Zampella, F. J., et al. (2011). *Simulation of foot-mounted IMU signals for the evaluation of PDR algorithms*. 2011 International Conference on Indoor Positioning and Indoor Navigation, IEEE.